Remote Sensing of Environment 115 (2011) 382–391

Contents lists available at ScienceDirect

Remote Sensing of Environment

journal homepage: www.elsevier.com/locate/rse

Monitoring fall foliage coloration dynamics using time-series satellite data

Xiaoyang Zhang [a,*], Mitchell D. Goldberg [b]

[a] Earth Resources Technology Inc. at NOAA/NESDIS/STAR, 5200 Auth Road, Camp Springs, MD 20746, United States
[b] NOAA/NESDIS/STAR, 5200 Auth Road, Camp Springs, MD 20746, United States

ARTICLE INFO

Article history:
Received 23 March 2010
Received in revised form 28 July 2010
Accepted 18 September 2010

Keywords:
Phenology
Fall foliage coloration
Foliage phase
Time-series satellite data
Temporally-normalized brownness

ABSTRACT

Fall foliage coloration is a phenomenon that occurs in many deciduous trees and shrubs worldwide. Measuring the phenology of fall foliage development is of great interest for climate change, the carbon cycle, ecology, and the tourist industry; but little effort has been devoted to monitoring the regional fall foliage status using remotely-sensed data. This study developed an innovative approach to monitoring fall foliage status by means of temporally-normalized brownness derived from MODIS (Moderate Resolution Imaging Spectroradiometer) data. Specifically, the time series of the MODIS Normalized Difference Vegetation Index (NDVI) was smoothed and functionalized using a sigmoidal model to depict the continuous dynamics of vegetation growth. The modeled temporal NDVI trajectory during the senescent phase was further combined with the mixture modeling to deduce the temporally-normalized brownness index which was independent of the surface background, vegetation abundance, and species composition. This brownness index was quantitatively linked with the fraction of colored and fallen leaves in order to model the fall foliage coloration status. This algorithm was tested by monitoring the fall foliage coloration phase using MODIS data in northeastern North America from 2001 to 2004. The MODIS-derived timing of foliage coloration phases was compared with in-situ measurements, which showed an overall absolute mean difference of less than 5 days for all foliage coloration phases and about 3 days for near peak coloration and peak coloration. This suggested that the fall foliage coloration phase retrieved from the temporally-normalized brownness index was qualitatively realistic and repeatable.

1. Introduction

Vegetation is one of the most important parameters in the determination of carbon cycles, water and energy balances, and climate and weather modeling (e.g., Anderson, 1997; Timmerman et al., 2007). Long-term annual variation in vegetation characteristics can effectively reflect anthropogenic effects on the biosphere and hydrosphere (e.g. Myneni et al., 1997; Zhang et al., 2007). In contrast, seasonal variation in vegetation foliage is particularly important in numerical weather prediction models (Gutman & Ignatov, 1998), hydrological models (Moreno-de las Heras et al., 2009), and land surface process models (Thornes, 1985; Zhang et al., 2002).

Seasonal vegetation growth basically experiences four phenological phases. These phases are the green-up phase, maturity phase, senescent phase, and dormant phase (Zhang et al., 2006). During the green-up phase, green-foliage cover generally increases from the minimum value in the dormant phase and reaches a maximum in the maturity phase. The fraction of green vegetation cover in a given period has been intensively investigated using satellite observations. Although green vegetation cover could be more appropriately estimated using polynomial regression or nonlinear models from the vegetation index (Purevdorj et al., 1998), linear empirical models are commonly applied (e.g., Nagler et al., 2004; Ormsby et al., 1987). Indeed, numerous linear models have been established between field-measured green vegetation cover in various vegetation types and the Normalized Difference Vegetation Index (NDVI) derived from various satellite instruments. Specifically, the AVHRR (Advanced Very High Resolution Radiometer) NDVI is correlated with the green vegetation fraction in deciduous forests (Blackburn & Milton, 1995; Wittich & Hansing, 1995), semiarid shrubland (Kennedy, 1989), and grassland (Purevdorj et al., 1998). The Landsat TM (Thematic Mapper) NDVI is associated with the green fraction in coniferous forests (Danson, 1989) and sugar beets (Malthus et al., 1993). Moreover, the MODIS (MODerate Resolution Imaging Spectroradiometer) NDVI is also strongly correlated with vegetation cover (Guerschman et al., 2009). These empirical models are applicable for quantitative estimates of the fraction of green vegetation cover for specific vegetation species, regions and satellite sensors. However, such models may be problematic for different ecosystems and sensors and they are not practicable or repeatable globally (Drake et al., 1999; Nagler et al., 2004). Such inconsistencies are caused by the variations in surface backgrounds (soil, rock, and litter), vegetation types, senescent vegetation, and sensor characteristics (Drake et al., 1999; Purevdorj et al., 1998; Xiao & Moody, 2005).

* Corresponding author.
E-mail address: xiaoyang.zhang@noaa.gov (X. Zhang).

0034-4257/$ – see front matter © 2010 Elsevier Inc. All rights reserved.
doi:10.1016/j.rse.2010.09.009

As the fraction of green vegetation cover decreases, colored foliage increases during the senescent phase in the fall. Fall foliage coloration is a phenomenon that occurs in many deciduous trees and shrubs worldwide. The most brightly colored fall foliage is found in mainland Canada, the United States, Scandinavia and Northern Europe, Russia and Eastern Asia. The complex mechanism of leaf color change has been examined by scientists in the fields of physiology, biochemistry, and molecular genetics (e.g., Buchanan-Wollaston et al., 2002; Feild et al., 2001; Lim et al., 2003; Schaberg et al., 2003). In addition, the phenological development of fall foliage has recently been monitored in fields by the USDA-Forest Service Regional Fall Foliage Sites (http://www.fs.fed.us/news/fallcolors/), forest-ecology networks (http://www.forestecologynetwork.org/), and citizen-scientist fall foliage networks (http://www.foliagenetwork.com/). Such observations are also broadcast by weather services (http://www.weather.com/) to public citizens in real time. Moreover, the long-term variations in fall foliage seasons have been demonstrated to be an effective index of global climate change (Myneni et al., 1997). However, while the start and the end of the foliage season have been investigated using satellite data (Reed et al., 1994; White et al., 1997; Zhang et al., 2003, 2006), little effort has been made to monitor the development of fall foliage coloration status using remote sensing.

It is widely recognized that retrieving the phenology of foliage status automatically from satellite data is a challenge. This is because vegetation signals in satellite data are often contaminated or blocked by the viewing and illumination geometry, atmosphere, cloud cover, snow cover, and complex background. This study developed an innovative approach to monitoring fall foliage status using a time series of temporally-normalized brownness derived from MODIS data. To do this, the time series of the MODIS NDVI in each pixel was smoothed and simulated using a sigmoidal model to obtain a temporally continuous trajectory during the senescent phase. By combining the temporal NDVI data and mixture modeling algorithm, a temporally-normalized brownness index was then deduced. This brownness was further used to quantitatively model the status of fall foliage coloration. This algorithm was used to calculate the fall foliage status across northeastern North America (MODIS land tile with horizontal 12 and vertical 4, 40°N–50°N and 65.3°W–93.3°W) from 2001 to 2004. Finally the results were assessed using a set of independent in-situ data.

2. Materials and methods

2.1. Field data on fall foliage development

Field measurements are critical for generating the criteria for satellite determination of foliage coloration and for assessing/validating the phenological results retrieved. In this study, field measurements of fall foliage development were obtained from both the Harvard Forest in central Massachusetts and the Hubbard Brook Experimental Forest in New Hampshire. The Harvard Forest is a long term ecological reserve (LTER) site located at 42°32'N and 72°11'W (http://www.lternet.edu/hfr/). This site records leaf development in 33 woody species representing most species of both overstory and understory individuals. The dominant species are red oak (*Quercus rubra*), red maple (*Acer rubrum*), black birch (*Betula lenta*), white pine (*Pinus strobus*), hemlock (*Tsuga canadensis*), white oak (*Quercus alba*), black oak (*Quercus velutina*), and hickory (*Carya ovata*), with a conifer cover of about 25% (http://public.ornl.gov/fluxnet/sitepage_data.cfm?SITEID=886#locdata). All individual species are located within 1.5 km of the Harvard Forest headquarters. The fall foliage observations include the percentage of leaves that have changed color on a given plant and the percentage of leaves that have fallen at 3- to 7-day intervals during the autumn.

We obtained data on fall foliage development at the Harvard Forest (http://www.lternet.edu/hfr/) from 2001 to 2008. To match these field measurements with satellite pixels, we calculated the average fraction of foliage cover at each observation time. The numerical average could realistically represent the foliage status in the vegetation community although it would be more appropriate to calculate the foliage phase based on the areal average if the percent area of each species were known.

Foliage measurements at the Hubbard Brook Experimental Forest (about 43°56'N and 71°43'W) are conducted by the USDA Forest Service in eight sites that are spatially-distributed in five small watersheds (http://www.hubbardbrook.org/data/dataset.php?id=51). The foliage development of the representative key tree species, which are American beech, sugar maple, and yellow birch, is measured in each site. The fall foliage status in each tree is measured weekly using a canopy development index with a scale ranging from 0 to 4. The criteria and index are: 4—only scattered leaves or branches changing color, 3—many leaves having noticeable reddening or yellowing, 2—most leaves becoming yellow or red, and a few fallen leaves, 1—no more green leaves on the canopy, half of the leaves fallen, 0.5—most leaves fallen. Individual observations usually record the timing and numerical values within the five levels.

We downloaded the fall foliage data from the Hubbard Brook Experimental Forest from 2001 to 2003. The timing corresponding to above five indices was calculated by linearly interpreting the numerical values of the index in the previous and succeeding observations.

These field measurements were used to develop the algorithm of foliage detection and to validate the results. Because the dataset from the Harvard Forest documents the detailed development of colored and fallen leaves in a vegetation community, the dataset from 2001 to 2004 was used to investigate the relationship between fall foliage status and the MODIS vegetation index (described in the following sections) while the dataset from 2005 to 2008 was used for validation purpose. The dataset at the Hubbard Brook Experimental Forest was only used to assess the foliage coloration phases retrieved from MODIS data because it was less accurately measured in field.

2.2. MODIS data and pre-processing

The primary satellite dataset collected in this study was a time series of MODIS data from 2001 to 2008 of northeastern North America (MODIS land tile H12V04, 40°N–50°N and 65.3°W–93.3°W), which was used to describe the phenology of fall foliage. Specifically, the MODIS dataset used here was the BRDF (bi-directional reflectance distribution function)/albedo product (MOD43B4, collection 5) with a spatial resolution of 500 m (Román et al., 2009; Schaaf et al., 2002). This dataset is operationally produced at an interval of 8 days using multi-day, cloud-free, and atmospherically-corrected surface reflectance from both Terra and Aqua to calculate the surface reflectance anisotropy over a 16-day period and to retrieve a reflectance anisotropy model for each pixel. The product generates the Nadir BRDF Adjusted Reflectance (NBAR) for MODIS bands 1–7. This NBAR dataset is temporally and spatially consistent and comparable. The MODIS BRDF/albedo product also provides a snow and ice flag in its Quality Assurance (QA) field, indicating whether the NBAR data are acquired from a snow-covered or snow-free surface. This snow and ice flag is inherited from the MODIS snow and ice products. Using this flag, spectral values contaminating snow properties can be explicitly discriminated.

We also used the MODIS land surface temperature (LST) product (MOD11A2, collection 5) from 2001 to 2008 in order to determine winter NBAR. The LST product produces estimates of the surface skin temperature for an 8-day time period by averaging the daily LST measurements with a spatial resolution of 1 km (Wan et al., 2002). The time series of LST for each pixel in this study was generated by replacing any missing values using a moving arithmetic average of the nearest preceding and subsequent values. It was then simply re-

sampled to a spatial resolution of 500 m using a nearest neighbour approach in order to match the MODIS NBAR data.

Preprocessing of the time series of NBAR data followed the algorithm described in Zhang et al. (2006). Briefly, we calculated a time series of NDVI from 8-day NBAR data in each pixel. This time series was then smoothed to fill missing values (because of cloud cover) and to eliminate spurious values. The missing values were replaced using a moving-window average of the two nearest good quality neighbors, where the moving-window began from the side with the higher NDVI value. The NDVI values with snow cover, which were identified using the QA flag, were replaced using the background (nearest snow-free) NDVI value. To further reduce the impact of partial snow and other background conditions during winter, which was determined using the LST of less than 5 °C, the irregular winter NDVI values were replaced with the nearest valid neighbor values in the time series.

Spurious values (or outliers), especially abnormally high NDVI values, were removed in the NDVI time series using a running median smoother. Specifically, the smoother calculated the median in a running window of three 8-day NDVI values to replace the middle value in the window. The process was applied interactively until there was no change in the time series. The time series of preprocessed NDVI was then employed to model the temporal trajectory of fall foliage development, which is depicted in detail in the following section.

2.3. Quantifying fall foliage development from satellite data

Seasonal variation in vegetation growth mainly occurs during the green-up phase and senescent phase. The most commonly used and simplified model for describing vegetation growth is the sigmoidal model. This model is capable of capturing the variation in vegetation leaf and biomass dynamics measured in both the field (Birch et al., 1998; Ratkowsky, 1983; Richards, 1959) and the satellite-derived vegetation index and leaf-area index (Ahl et al., 2006; Zhang et al., 2003). The temporal variation in satellite-derived vegetation greenness (NDVI) data for a senescent phase can be modeled using a function of the form (Zhang et al., 2003):

$$y_{(t)} = \frac{c}{1 + e^{a + bt}} + d \tag{1}$$

where t is time in days, $y_{(t)}$ is the NDVI value at time t, a and b are parameters characterizing the rate of development of senescence, $c+d$ is the maximum NDVI value, and d is the initial background NDVI value.

The NDVI value in a pixel is assumed to be a linear mixture of surface components. The land surface is basically covered by green (or photosynthetic) vegetation, colored (or non-photosynthetic) vegetation, and exposed surface background (mainly bare soil and rock). The fractions of these three components in a given pixel can be assumed to contribute to the spectral reflectance (e.g., Adams et al., 1986; Drake, 1991; Smith et al., 1990) and NDVI (e.g., Busetto et al., 2008; Gutman & Ignatov, 1998; Kerdiles & Grondona, 1995; Maselli, 2001; Xiao & Moody, 2005) in a linear combination. If the shadow impact is assumed to be insignificant and negligible, the NDVI values in an individual pixel can be described using a mixture modeling:

$$\begin{cases} y_{(t)} = F_{g(t)}y_g + F_{c(t)}y_c + F_{b(t)}y_b + \varepsilon \\ F_{g(t)} + F_{c(t)} + F_{b(t)} = 1 \end{cases} \tag{2}$$

where F_g, F_c, and F_b are the fractions of green vegetation, colored vegetation, and exposed surface background, respectively; y_g, y_c, and y_b are the end-members of the NDVI values for the above three components, and ε is the residual error, which can be assumed to be zero.

As the NDVI values in the colored leaves (~0.14) and exposed surface background (~0.1) are less distinguishable, but contrast with the NDVI in green vegetation (~0.72) (http://earthobservatory.nasa.gov/Features/MeasuringVegetation/; Gutman & Ignatov, 1998; Wittich & Hansing, 1995), the land-surface components can be simplified as green material and brown material. Thus, the mixture modeling in Eq. (2) can be simplified as:

$$\begin{cases} y_{(t)} = F_{g(t)}y_g + F_{cb(t)}y_{cb} \\ F_{g(t)} + F_{cb(t)} = 1 \end{cases} \tag{3}$$

where $F_{cb(t)}$ $(=F_{c(t)}+F_{b(t)})$ and y_{cb} are the fraction and NDVI end-member of the brown material, respectively.

The fraction of colored foliage is the parameter that is used in the determination of fall foliage status. However, this fraction varies with pixels or vegetation communities due to both the plant abundance and the mixture of evergreen and deciduous plants. To make fall foliage status comparable spatially and temporally, we proposed an index of temporally-normalized brownness to describe the relative dynamics of the fraction of colored foliage. During the senescent phase in a given pixel, we assumed that (1) the minimum fraction of colored leaves (F_{cmin}) occurs just before the onset of senescence, which approximates zero ($F_{cmin}\approx 0$); (2) the fraction of the colored leaf cover includes leaves both on the plant canopy and on the ground, as they have similar spectral properties; (3) the fraction and NDVI value of the exposed surface background, which mainly refers to bare soils and rocks that are never covered by vegetation canopy during the senescent phase, are constant. Therefore, the temporally-normalized brownness index can be described as:

$$NF_{b(t)} = \frac{F_{c(t)} - F_{c\min}}{F_{c\max} - F_{c\min}} = \frac{\left(F_{cb(t)} - F_b\right) - \left(F_{cb\min} - F_b\right)}{\left(F_{cb\max} - F_b\right) - \left(F_{cb\min} - F_b\right)} = \frac{F_{cb(t)} - F_{cb\min}}{F_{cb\max} - F_{cb\min}} \tag{4}$$

where $F_{cb\min} = F_{c\min} + F_b$; $F_{cb\max} = F_{c\max} + F_b$; $F_{cb(t)} = F_{c(t)} + F_b$; $NF_{b(t)}$ is defined as the temporally-normalized brownness at time t; $F_{c(t)}$ and $F_{cb(t)}$ are the fraction of colored vegetation and brown material at time t, separately; $F_{c\min}$ and $F_{c\max}$ are the minimum and maximum fractions of colored leaf cover; and $F_{cb\min}$ and $F_{cb\max}$ are the minimum and maximum fractions of brown material during the senescent phase, seperately.

The $F_{cb\min}$ and $F_{cb\max}$ can be derived from Eqs. (1) and (3):

$$F_{cb\max} = \lim_{t\to\infty} F_{cb(t)} = \frac{d - y_g}{y_{cb} - y_g} \tag{5}$$

$$F_{cb\min} = \lim_{t\to 0} F_{cb(t)} = \frac{c + d - y_g}{y_{cb} - y_g} \tag{6}$$

By combining Eqs. (1), (3)–(6), we can derive the formula for the temporally-normalized brownness index:

$$NF_{b(t)} = 1 - \frac{1}{1 + e^{a + bt}} \tag{7}$$

The temporally-normalized brownness index represents relative changes in colored foliage and varies with time in each pixel individually. Its temporal trajectory is independent of the fraction of colored leaves and exposed surface background and is only characterized by leaf development parameters a and b. These two parameters in each pixel are calculated by fitting the time series of the MODIS NDVI data during the senescent phase using Eq. (1). Thus, the temporally-normalized brownness index allows us to compare the foliage development across heterogeneous ecosystems over a wide area regardless of the heterogeneity in plant species, abundance, and surface properties.

2.4. Modeling fall foliage phase using temporally-normalized brownness index

The temporally-normalized brownness index is quantitatively associated with fall foliage phase. The fall foliage phase is generally classified into several categories according to the percentage of colored leaves. Based on field observations, the United States Weather Channel (http://www.weather.com/) defines the fall foliage color status as: no change (0–10% colored leaves), patchy (10–50% colored leaves), near-peak (50–75% colored leaves), peak (75–100% colored leaves), and post-peak. The foliage network (http://www.foliagenetwork.net/) also uses certain thresholds of the percentage of colored leaves to classify fall foliage color status as little/no change, low color, moderate color, high color, peak color, and post-peak color.

The foliage phase in this study was quantified using models based on the temporally-normalized brownness index and the percentages of colored leaves and fallen leaves. These models were established using field observations (described in Section 2.1) in the Harvard Forest during 2001–2004 and the temporally-normalized brownness index derived from MODIS data. Specifically, the temporal MODIS NDVI data were used to fit function (1) for each year, separately. The fitted function was converted to the temporal trajectory of the normalized brownness index using Eq. (7). Using the temporally-normalized brownness index as the independent variable, empirical models for predicting colored leaves and fallen leaves were established, separately.

The fall foliage phase was classified by combining the categories used in both the Weather Channel (http://www.weather.com/) and the foliage network (http://www.foliagenetwork.net/) and the models of both colored leaves on a plant canopy and fallen leaves. As the percentage of fallen leaves increases with the spread of colored foliage, the occurrence of their maximum difference is considered to be a critical point in foliage coloration status. Prior to this critical point, the foliage phase is referred as to little/no change, low coloration, moderate coloration, and near-peak coloration. Following the critical point, it is defined as peak coloration and post-peak coloration.

This algorithm was applied to detect the fall foliage status in northeast North America using time series of NDVI calculated from MODIS NBAR data from 2001 to 2004. The results and algorithms were assessed using independent field measurements from the Hubbard Brook Experimental Forest and the Harvard Forest.

3. Results

3.1. Variation in ground measurements of foliage coloration

The percentage of colored and fallen leaves among individual plants varied considerably for a given date during the senescent phase at the Harvard Forest from 2001 to 2004. At early September, the standard deviation of the percent colored leaves (%) on different plants was less than 10. It increased to about 35 in mid October, which indicated that leaves were all changed color in some plants while they were mostly green in others. The standard deviation became less than 5 in the end of October, where few green leaves remained on the canopy. A similar pattern appeared in the fallen leaves. The timing for a given percentage of colored leaves was also different greatly among various species. For example, the timing at which 60% of leaves were colored in individual plants ranged from DOY (day of year) 276 to 288 in 24 species in 2001, while in other species this stage was reached as early as DOY 250 or as late as DOY 295.

The average timing of occurrence of foliage phases differed inter-annually at the Harvard Forest. During the period of 2001–2004, the standard deviation of the timing was 2.8, 1.7, 2.2, and 3.6 days for the average percentage of colored leaves of 20%, 40%, 60%, and 80%, respectively. Similarly, the standard deviation was 2.2, 4.1, 4.6, and 4.5 days for the average percentage of fallen leaves of 20%, 40%, 60%, and 80%, respectively (Fig. 1). The inter-annual variation was also noticeable in the Hubbard Brook Experimental Forest. The standard deviation of timing corresponding to the foliage status of 4, 3, 2, 1, and 0.5 during 2001–2003 was 5.6, 4.0, 3.0, 5.0, and 6.6 days, respectively.

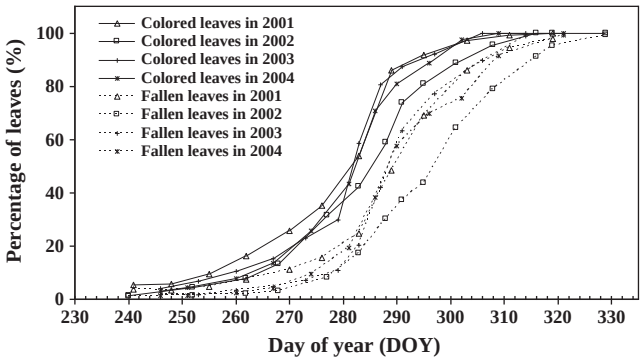

Fig. 1. Field measurements of colored leaves and fallen leaves from 2001 to 2004 at the Harvard Forest.

3.2. Fall foliage phase based on temporally-normalized brownness index

The percentage of colored foliage and fallen leaves is a function of the temporally-normalized brownness index (Fig. 2). The models based on data from the Harvard Forest (2001–2004) are expressed as:

$$CF_{(t)} = 105.48NF_{b(t)} \qquad CF_{(t)} = 100 \quad \text{if } CF_{(t)} > 100 \left(r^2 = 0.99, p<0.0001\right) \tag{8}$$

$$DF_{(t)} = -9.774\left(1-e^{2.44NF_{b(t)}}\right) \quad DF_{(t)} = 100 \quad \text{if } DF_{(t)} > 100 \left(r^2 = 0.96, p<0.0001\right) \tag{9}$$

where CF is the percentage of colored leaves, DF is the percentage of fallen leaves, NF_b is the temporally-normalized brownness index, and t is time.

The models are realistic in describing the foliage status. When NF_b is zero, both the colored and fallen leaves are also zero without an intercept. The percentage of fallen leaves increases exponentially with

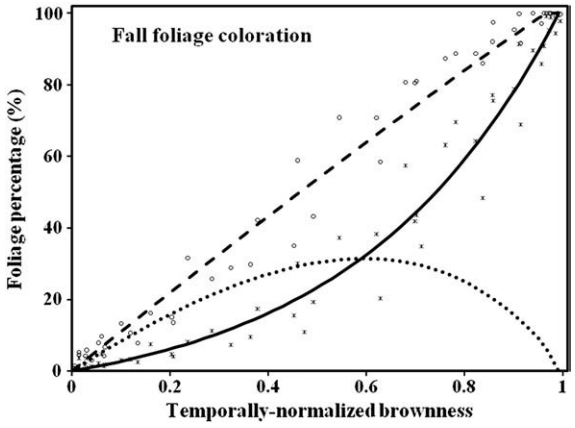

Fig. 2. Correlation of the temporally-normalized brownness index with the colored leaves and fallen leaves, separately. The circles are samples of percent colored leaves; the asterisks are samples of fallen leaves; the dashed line is the relationship between percent colored foliage and temporally-normalized brownness index as described in Eq. (8); the solid line is the relationship between percent fallen foliage and temporally-normalized brownness index as described in Eq. (9); and the dotted line represents the variation in the difference between percent colored foliage and fallen foliage.

the normalized brownness index and reaches 100% when the NF_b is 1. In contrast, the percentage of colored leaves increases linearly and reaches 100% when the NF_b is about 0.96.

The difference between the colored leaves and the fallen leaves ($dCDF_{(t)} = CF_{(t)} - DF_{(t)}$) is an index representing the status of the colored leaves on the plant canopy. The *dCDF* increases gradually and then decreases with the increase in NF_b (Fig. 2). The peak along the temporal *dCDF* occurs when NF_b reaches about 0.61, at which point the percentage of colored foliage is 65% and that of the fallen leaves is 34%. This critical point is defined as the start of peak coloration, where the corresponding NF_b is simply rounded to 0.60. Prior to this point, the NF_b is linearly divided into three parts. The first part is further linearly divided into little coloration and low coloration. The second and third parts are corresponding to moderated correlation and near-peak coloration, respectively. Similarly, the peak coloration and post-peak coloration are separated according to NF_b values. The corresponding colored and fallen leaves are determined based on Eqs. (8) and (9) (Table 1).

3.3. Spatial pattern in fall foliage phases in northeastern North America

The fall foliage phase during 2001–2004 was produced using the temporally-normalized brownness index derived from MODIS data in northeastern North America. The standard deviation of data during the four years is relatively small for the timing of onset of the peak and near-peak colorations compared with that for other phases. The inter-annual variation in the timing of peak and near-peak colorations is less than 10 days in more than 90% of the region (Fig. 3). This result is comparable with the inter-annual variation in field measurements as described in Section 3.1, which also demonstrates that the developed algorithm is consistent and repeatable.

Fig. 4 presents the spatial pattern in the timing of onset of fall foliage status across the study region. As expected, the basic pattern reveals a gradual shift from north to south with variation in latitude. This pattern matchs well with Hopkins Law of the effects of temperature on vegetation phenology (Hopkins, 1938). It suggests that temperature is likely the main forces driving fall foliage variations at large regions although plant species may have significant contributions to the local variation in foliage colorations. However, foliage coloration also varies with longitude, although no regular pattern has been discovered. This spatial heterogeneity is likely associated mainly with the pattern of local climate, elevation, and plant species.

Fig. 5 quantifies the timing of foliage coloration as a zonal average along latitude for natural vegetation (croplands are excluded). Low foliage coloration begins in early September around DOY 250 at 45–50°N, gradually spreads southward, and appears at 40°N in mid September (around DOY 260). The peak foliage coloration occurs at the end of September (DOY 270) in the north and in mid October (DOY 290) in the south. This exhibits a gradient of 2.7 days per latitude degree. Similar spatial patterns occur for other foliage coloration phases.

The duration of each foliage coloration phase also varies with latitude (Fig. 6). From 50°N to 40°N, low coloration lasts about 5–10 days, moderate coloration 8–11 days, near-peak 7–9 days, peak coloration 10–15 days, and post-coloration 8–12 days. The gradient calculated from the linear regression analysis shows that the duration of foliage phases decreases northwards with a gradient of 0.66, 0.42, 0.31, 0.50, and 0.46 days per latitude degree for low coloration, moderate coloration, near-peak coloration, peak coloration, and post-peak coloration, respectively. The largest gradient occurs in the low coloration phase while the smallest gradient appears in the near-peak coloration phase.

Table 1
Criteria for determining fall foliage phase from the temporally-normalized brownness index.

Fall foliage phase	NF_b	CF	DF
Little/no coloration	0–0.1	0–11	0–3
Low coloration	0.1–0.2	11–21	3–6
Moderate coloration	0.2–0.4	21–42	6–16
Near-peak coloration	0.4–0.6	42–63	16–32
Peak coloration	0.6–0.85	63–90	32–68
Post-peak coloration	0.85–1	90–100	68–100

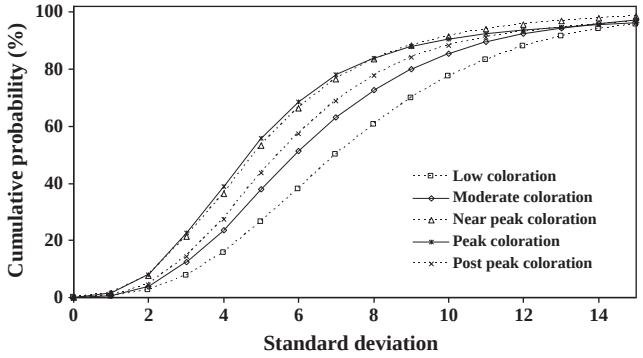

Fig. 3. Cumulative probability of inter-annual variation (2001–2004) in the timing of onset of each foliage coloration phase across northeastern North America.

3.4. Evaluation of MODIS fall foliage coloration using in-situ measurements

The fall foliage phase predicted using the MODIS data was assessed using in-situ data from the Hubbard Brook Experimental Forest and the Harvard Forest. Validation of remote sensing retrievals is an important but difficult task. First, MODIS observes the fall foliage in a vegetation community within an entire 500 m footprint whereas the field data measure several representative plants (three tree species in the Hubbard Brook Experimental Forest). Second, the MODIS pixels at 500 m contain geo-location uncertainties (Tan et al., 2006) and may not match well with field points. Third, NBAR NDVI with 8-day intervals is a model value within a 16-day period, which may also lead to potential error. Fourth, the quality of the field measurements is also greatly affected by the experience of the data collector. In particular, the foliage color index in the Hubbard Brook Experimental Forest is based on experience rather than an accurate instrumental measurement, which commonly results in an error of several days. Bearing these problems in mind, it would be more appropriate to evaluate the variance between field measurements and satellite retrievals rather than to validate the satellite retrievals. If the difference between the two datasets is within the temporal span (seven days here) of field observations, the satellite-derived product could be considered acceptable.

Fig. 7 presents the five phases of fall foliage development in eight sites of the Hubbard Brook Experimental Forest. Because each foliage phase covers a certain time period, the middle day of each foliage phase obtained from the MODIS retrieval was compared with that of the five phases observed in the Hubbard Brook Experimental Forest. If each field measurement (three tree species) is plotted against the MODIS retrieval of the corresponding 500 m pixel, the samples are generally located along a 1:1 line in each year with a significant correlation ($p<0.0001$) although the samples are relatively scattered during early and late coloration phases in 2002 (Fig. 7a). The absolute mean difference (AMD) in all sample pairs is 5.1 days in 2001, 8.3 days in 2002, and 4.3 days in 2003. However, the AMD difference in the near-peak and peak coloration is 4.7 days, 4.7 days, and 3.9 days during the three years, respectively. If the average of each foliage phase from the eight sites is compared with the average of the corresponding MODIS pixels, which reduces mismatches related to

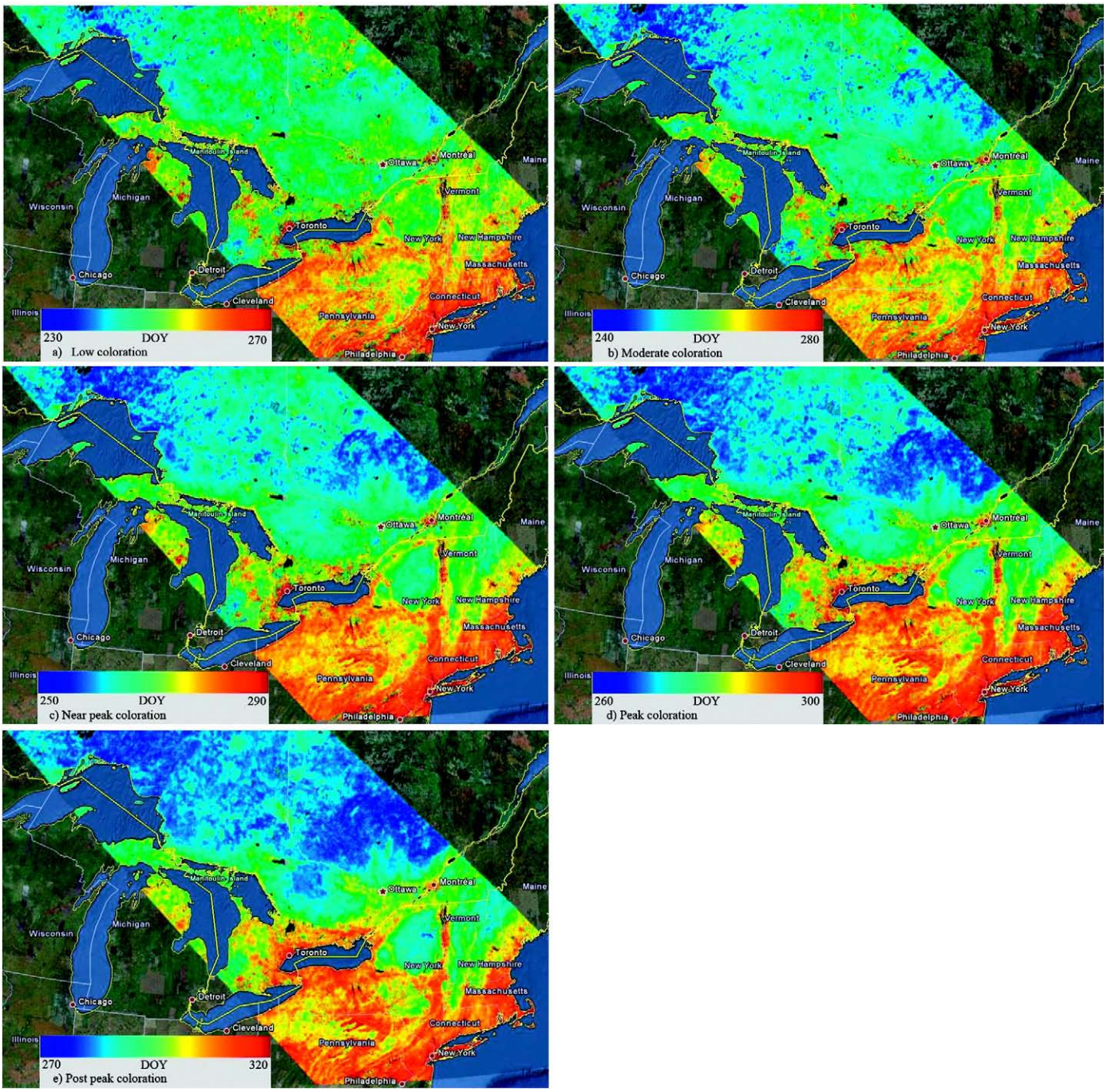

Fig. 4. Spatial pattern in the timing of onset of foliage coloration phases averaged from 2001 to 2004 in northeastern North America (MODIS tile H12V04, a spatial resolution of 500 m). a) Onset of low coloration; b) onset of moderate coloration; c) onset of near peak coloration; d) onset of peak coloration; and e) post peak coloration.

geo-location and increases the representatives of the vegetation community, the MODIS retrievals are similar to in-situ measurements, with a AMD difference of 4.7 days (3.4 days at near-peak and peak coloration) (Fig. 7b). This demonstrates that the difference between the MODIS retrievals and field measurements is smaller than the time span of the field measurements (7 days) and suggests that the MODIS-derived fall foliage phase, especially the near-peak and peak colorations, is acceptable overall.

Fig. 8 exhibits the timing of occurrence of fall foliage phases (except little/no coloration) for both in-situ measurements and MODIS detections from an independent dataset at the Harvard Forest from 2005 to 2008. The result shows that these two datasets are closely distributed along a 1:1 line with a slope of 1.02. The MODIS retrieval can explain 95% of the variation measured in field. The AMD difference between these two datasets is about 3 days. Moreover, inter-annual comparison shows the MODIS-derived start timing of five foliage coloration phases on average in 2005 is 10.2, 2.6 and 5.2 days later than that in 2006, 2007 and 2008, respectively. This matches very well with the in-situ measurements that the start timing in 2005 is 9.6, 4.4 and 4.4 days later than that in 2006, 2007 and 2008, respectively.

4. Discussion

The results presented here represent a first attempt at using a time series of satellite data to monitor the fall foliage coloration phases.

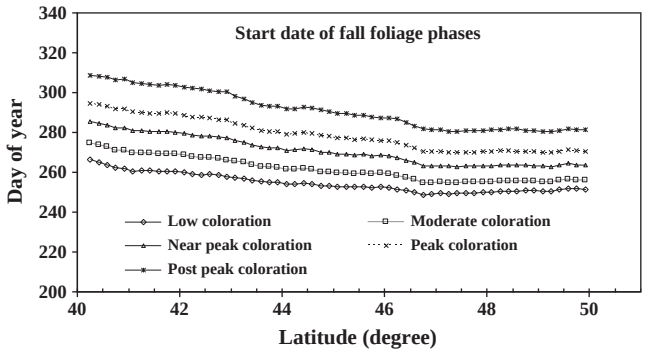

Fig. 5. Timing of onset of each foliage coloration phase with latitude.

Below we discuss the overall performance of the temporally-normalized brownness index in the detection of foliage coloration phases and the potential uncertainties and limitations of the proposed approach.

The temporally-normalized brownness index is principally defined using temporal NDVI variation and mixture modeling. This study simulates temporal NDVI trajectory using a sigmoidal model in capturing the continuous development of foliage senescent phases, although the temporal trajectory can also be generated using various approaches including Fourier analysis (Moody & Johnson, 2001), asymmetric Gaussian function-fitting (Jönsson & Eklundh, 2002), degree-day based quadratic model (de Beurs & Henebry, 2004), and polynomial curve fitting (Bradley et al., 2007). The advantages of the sigmoidal model include that each parameter has its biophysical meaning in describing vegetation growth and that the model has been widely tested based on field measurements, webcam vegetation index, and satellite data (e.g., Ahl et al., 2006; Birch et al., 1998; Ratkowsky, 1983; Richards, 1959; Richardson et al., 2006; Zhang et al., 2003). Moreover, the sigmoidal model performances better than both the Fourier functions and the asymmetric Gaussian functions in fitting MODIS NDVI curve (Beck et al., 2006). However, the accuracy of sigmoidal model in a given pixel could be influenced by the cloud contaminations in the time series of MODIS data and the temporal representative of NBAR NDVI values modeled from 16-day BRDF (Zhang et al., 2009). This could cause some uncertainties in detecting fall foliage phases, so that the detection confidence in each pixel should be assessed in future.

The relative fraction of colored leaves is derived from linear mixture modeling of vegetation index. Theoretically, spectral reflectance within a pixel is the nonlinear combinations of surface cover fractions if the incident flux reacts with more than one component before being reflected from the surface (Johnson et al., 1985; Mustard & Pieters, 1987). In contrast, if there is not a significant amount of multiple scattering of a photon between the surface materials, the flux received by remote sensor is combined in an additive fashion (García-Haro et al., 1996). Although linearity in the composition of the surface components in a pixel is strictly valid only for the original spectral reflectance (Lobell & Asner, 2004), the linearity assumption of NDVI only leads to a very minor inaccuracy (Busetto et al., 2008; Kerdiles & Grondona, 1995). Therefore, the approach of linear NDVI mixture modeling is widely applied in extracting the fractions of vegetation and land cover effectively (e.g., Busetto et al., 2008; Gutman & Ignatov,

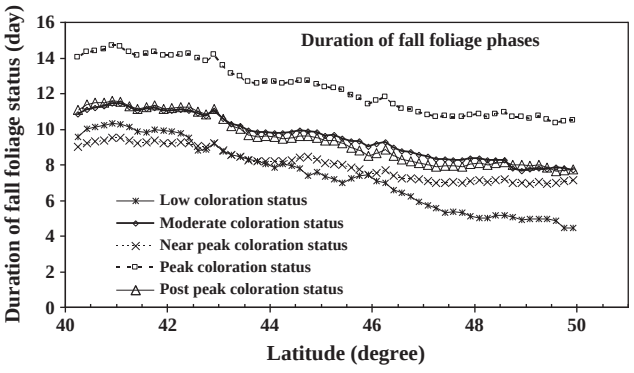

Fig. 6. Duration of each foliage coloration phase with latitude.

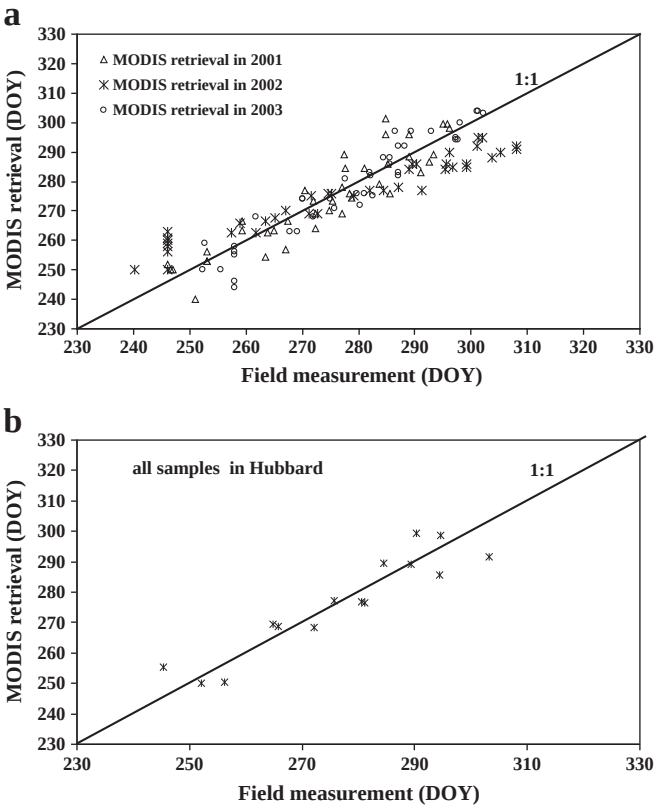

Fig. 7. Comparison of the start timing of fall foliage coloration phases between in-situ measurements (eight small sites) and MODDIS retrievals in the Hubbard Brook Experimental Forest. A) Observations from each site against the corresponding MODIS 500 m pixel; b) average observations from eight sites against the average of the corresponding MODIS pixels.

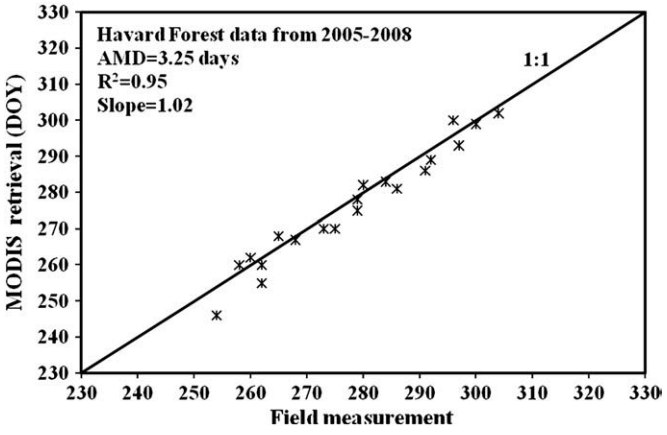

Fig. 8. Comparison of the start timing of fall foliage coloration phases between in-situ measurements and MODIS retrievals at the Harvard Forest from 2005 to 2008. AMD is the absolute mean difference.

1998; Kerdiles & Grondona, 1995; Maselli, 2001; Qi et al., 2000; Xiao & Moody, 2005; Zeng et al., 2000). The advantage of this algorithm is that linear mixture modeling can transform NDVI (or reflectance) data into fractions of a few dominant materials of interest in a pixel and can easily produce reasonable results (Adams et al., 1986; Busetto et al., 2008; Settle & Drake, 1993; Smith et al., 1985, 1990; Tompkins et al., 1997). In this study, we are aware of the theoretical nonlinearity of the NDVI combination of different surface components within a pixel. However, the linear NDVI mixture analysis allows us to deduce the temporal variation in the relative fraction of colored leaves, which lead to the developments of temporally-normalized brownness index.

The temporally-normalized brownness index measures the relative variation in colored leaves within a pixel. This index varies from 0 before the onset of senescence to 1 after the onset of dormancy, which is independent of the area of surface components and the types of plant species. Thus, the six fall foliage coloration phases determined from the temporally-normalized brownness should be spatially comparable. However, the criteria in classifying the six coloration phases, particularly the start of peak coloration phase, are currently based on the empirical models established from limited ground measurements in the Harvard Forest. Therefore, the uncertainty of the criteria should be further evaluated using a large number of ground sites from various ecosystems and plant species in future.

The phases of fall foliage coloration detected in this study represent the foliage development of vegetation communities in an entire MODIS pixel. It is currently impossible for us to distinguish species-specific fall foliages and to separate tree canopy foliages from understory vegetation (Ahl et al., 2006; Ahrends et al., 2008). If a pixel contains plants with very different seasonal cycles, the MODIS retrievals represent the overall foliage coloration phases within the pixel, which does not necessarily match well with the coloration in any individual species. However, if a pixel is dominated by species with similar senescent phases, the MODIS-derived foliage phases could represent well the species-specific foliage development.

Spatial pattern in foliage coloration phases is complex across our study region. Because the timing of foliage coloration varies greatly among different species within a pixel, such as Harvard Forest, spatial distribution in dominating plant species may play a significant role in the spatial variation in foliage coloration. Until reliable species distribution data are available, it is difficult to quantify the degree of species impacts. However, at large regions in mid-high latitudes, phenology gradient along latitude is likely controlled by temperature variation (e.g., Hopkins, 1938; Schwartz & Reiter, 2000; Zhang et al., 2004).

Finally, validation of satellite phenology is one of the most important and challenging parts. Assessment of MODIS retrievals using limited field observations at the Harvard Forests and the Hubbard Brook Experimental Forest indicates that the developed algorithm can monitor well the timing of foliage coloration phases and their inter-annual variation with an overall accuracy of 3–5 days. To sufficiently evaluate the accuracy of the detected coloration phases across the study region, more field measurements are needed, particularly field measurements from various ecosystems and plant species. However, direct validation of MODIS foliage coloration phases has been limited by a lack of in-situ observations sufficient to account for spatial heterogeneity and to represent vegetation community (Ganguly et al., 2010; Liang & Schwartz, 2009; Reed et al., 2009; Schwartz & Hanes, 2009). It has been recognized that reconciliation of the ground and satellite-based phenological observations is extremely challenging and that in-situ datasets collected across ecosystems at spatial scales commensurate with MODIS data are urgently required (de Beurs & Henebry, 2010; Ganguly et al., 2010; Liang & Schwartz, 2009; Morisette et al., 2009; Reed et al., 2009; Schwartz & Hanes, 2009; White et al., 2009; Zhang et al., 2006). Substantial validation in future is possible by up-scaling intensive field phenology measurements to vegetation community and landscape scales (Liang & Schwartz, 2009) and observing vegetation variation continuously using webcams (Richardson et al., 2009).

5. Conclusions

This paper presents, for the first time, a temporally-normalized brownness index for detecting the phases of fall foliage coloration using remotely sensed data. This new algorithm functionalizes the temporal trajectory of vegetation brownness using temporally normalized values. In this way, the temporal variation is described using a mathematical formula that is able to minimize the irregular variation in the remotely-sensed vegetation index. Furthermore, the algorithm of temporal normalization eliminates the effects on the detection of fall foliage development caused by the different vegetation proportions, complexity of vegetation species, and heterogeneity of the surface background within pixels.

By linking the MODIS trajectory of the temporally-normalized brownness index to field data on colored and fallen leaves, this paper further proposes criteria for categorizing the six phases of fall foliage colorations that are little coloration, low coloration, moderation coloration, near-peak coloration, peak coloration, and post-peak coloration. Although accurate validation is difficult in remotely sensed products, the MODIS detection of fall foliage phases has been evaluated using independent in-situ data. The overall absolute mean difference between them during entire coloration phases is 3.3 days at the Harvard Forest and 4.7 days at the Hubbard Brook Experimental Forest where the difference is 3.4 days in the near-peak and peak coloration phases. Because of the uncertainties in field measurements, the difference does not imply errors in the MODIS retrievals. This result instead suggests that the MODIS monitoring is realistic and comparable with field observations.

The results from 2001 to 2004 in northeastern North America suggest that the detection of fall foliage status using MODIS data is geographically and ecologically realistic and that the algorithm is repeatable and consistent. Specifically, the foliage phase shows a consistent spatial pattern that is delayed from north to south. The inter-annual variation is comparable to the variation in field observations, which suggests that long-term fall foliage detections could reveal the trends of climate changes.

In summary, it is evident that the developed method is capable of identifying foliage coloration phases in various ecosystems and regions. While this work provides a potential tool to monitor and forecast the status of foliage coloration, future works are needed to evaluate the algorithm and to validate the results using a large number of ground measurements from various ecosystems and plant species.

Acknowledgements

This work was partially supported by NOAA contract DG133E-06-CQ-0030. The authors thank Crystal B. Schaaf for help in MODIS NABAR data. We also wish to thank John O'Keefe at the Harvard Forest LTER and Amey Bailey of the USDA Forest Service Hubbard Brook Experimental Forest for providing phenology data, and anonymous reviewers for valuable comments. The views, opinions, and findings contained in this study are those of the author(s) and should not be interpreted as an official NOAA or US Government position, policy, or decision.

References

Adams, J. B., Smith, M. O., & Johnson, P. E. (1986). Spectral mixture modeling: A new analysis of rock and soil types at the Viking Lander 1 site. *Journal of Geophysical Research*, *91*(B8), 8098−8112.

Ahl, D. E., Gower, S. T., Burrows, S. N., Shabanov, N. V., Myneni, R. B., & Knyazikhin, Y. (2006). Monitoring spring canopy phenology of a deciduous broadleaf forest using MODIS. *Remote Sensing of Environment*, *104*(1), 88−95.

Ahrends, H. E., Brügger, R., Stöckli, R., Schenk, J., Michna, P., Jeanneret, F., et al. (2008). Quantitative phenological observations of a mixed beech forest in northern Switzerland with digital photography. *Journal of Geophysical Research*, *113*, G04004. doi:10.1029/2007JG000650.

Anderson, M. A. (1997). A two-source time-integrated model for estimating surface fluxes using thermal infrared remote sensing. *Remote Sensing of Environment*, *60*, 195−216.

Beck, P. S. A., Atzberger, C., Høgda, K. A., Johansen, B., & Skidmore, A. K. (2006). Improved monitoring of vegetation dynamics at very high latitudes: A new method using MODIS NDVI. *Remote Sensing of Environment*, *100*, 321−334.

Birch, C. J., Hammer, G. L., & Rickert, K. G. (1998). Improved methods for predicting leaf area and leaf senescence in maize (*Zea mays*). *Australian Journal of Agricultural Research*, *49*, 249−262.

Blackburn, G. A., & Milton, E. J. (1995). Seasonal variations in the spectral reflectance of deciduous tree canopies. *International Journal of Remote Sensing*, *16*, 709−721.

Bradley, B. A., Jacob, R. W., Hermance, J. F., & Mustard, J. F. (2007). A curve fitting procedure to derive inter-annual phenologies from time series of noisy satellite NDVI data. *Remote Sensing of Environment*, *106*, 137−145.

Buchanan-Wollaston, V., Earl, S., Harrison, E., Mathas, E., Navabpour, S., Page, T., et al. (2002). The molecular analysis of leaf senescence—A genomics approach. *Plant Biotechnology Journal*, *1*(1), 3−22.

Busetto, L., Meroni, M., & Colombo, R. (2008). Combining medium and coarse spatial resolution satellite data to improve the estimation of sub-pixel NDVI time series. *Remote Sensing of Environment*, *112*, 118−131.

Danson, F. M. (1989). *Factors affecting the remotely-sensed response of coniferous forest canopies*, Ph.D. Thesis, University of Sheffield.

de Beurs, K. M., & Henebry, G. M. (2004). Land surface phenology, climatic variation, and institutional change: Analyzing agricultural land cover change in Kazakhstan. *Remote Sensing of Environment*, *89*, 497−509.

de Beurs, K. M., & Henebry, G. M. (2010). Spatio-temporal statistical methods for modeling land surface phenology. In I. L. Hudson, & M. R. Keatley (Eds.), *Phenological research*. : C_ Springer Science+Business Media B.V. doi:10.1007/978-90-481-3335-2_9.

Drake, N. A. (1991). Mapping rocks, soil, vegetation communities and vegetation density with the GERIS using linear mixture modeling and post-processing techniques. *Earsel Advances in Remote Sensing*, *1*(1), 48−57.

Drake, N. A., Mackin, S., & Settle, J. J. (1999). Mapping vegetation, soils, and geology in semiarid shrublands using spectral matching and mixture modeling of SWIR AVIRIS imagery. *Remote Sensing of Environment*, *68*, 12−25.

Feild, T. S., Lee, D. W., & Holbrook, N. M. (2001). Why leaves turn red in autumn. The role of anthocyanins in senescing leaves of red-osier dogwood. *Plant Physiology*, *127*, 566−574.

Ganguly, S., Friedl, M. A., Tan, B., Zhang, X., & Verma, M. (2010). Land surface phenology from MODIS: Characterization of the Collection 5 Global Land Cover dynamics product. *Remote Sensing of Environment*, *114*(8), 1805−1816. doi:10.1016/j.rse.2010.04.005.

García-Haro, F. J., Gilabert, M. A., & Meliá, J. (1996). Linear spectral mixture modelling to estimate vegetation amount from optical spectral data. *International Journal of Remote Sensing*, *17*(17), 3373−3400.

Guerschman, J. P., Hill, M. J., Renzullo, L. J., Barrett, D. J., Marks, A. S., & Botha, E. J. (2009). Estimating fractional cover of photosynthetic vegetation, non-photosynthetic vegetation and bare soil in the Australian tropical savanna region upscaling the EO-1 Hyperion and MODIS sensors. *Remote Sensing of Environment*, *113*(5), 928−945.

Gutman, G., & Ignatov, A. (1998). The derivation of the green vegetation fraction from NOAA/AVHRR data for use in numerical weather prediction models. *International Journal of Remote Sensing*, *19*, 1533−1543.

Hopkins, A. D. (1938). Bioclimatics—A science of life and climate relations. *US Department of Agriculture Misc. Publication No. 280*. US Government Printing Office, Washington, DC.

Johnson, P. E., Smith, M. O., & Adams, J. B. (1985). Quantitative analysis of planetary reflectance spectra with principal components analysis. *Journal of Geophysical Research*, *90*, C805−C810.

Jönsson, P., & Eklundh, L. (2002). Seasonality extraction by function fitting to time-series of satellite sensor data. *IEEE Geosciences and Remote Sensing*, *40*, 1824−1831.

Kennedy, P. J. (1989). Monitoring the vegetation of Tunisian grazing lands using the normalized difference vegetation index. *Ambio*, *18*, 119−123.

Kerdiles, H., & Grondona, M. O. (1995). NOAA-AVHRR NDVI decomposition and subpixel classification using linear mixing in the Argentinean Pampa. *International Journal of Remote Sensing*, *16*, 1303−1325.

Liang, L., & Schwartz, M. (2009). Landscape phenology: An integrative approach to seasonal vegetation dynamics. *Landscape Ecology*, *24*(4), 465−472.

Lim, P. O., Woo, H. R., & Nam, H. G. (2003). Molecular genetics of leaf senescence in *Arabidopsis*. *Trends in Plant Science*, *8*(6), 272−278.

Lobell, D. B., & Asner, G. P. (2004). Cropland distributions from temporal unmixing of MODIS data. *Remote Sensing of Environment*, *93*, 412−422.

Malthus, T. J., Andrieu, B., Danson, F. M., Jaggard, K. W., & Steven, M. D. (1993). Candidate high spectral resolution infrared indices for crop cover. *Remote Sensing of Environment*, *46*, 204−212.

Maselli, F. (2001). Definition of spatially variable spectral endmembers by locally calibrated multivariate regression analyses. *Remote Sensing of Environment*, *75*, 29−38.

Moody, A., & Johnson, D. M. (2001). Land-surface phenologies from AVHRR using the discrete Fourier transform. *Remote Sensing of Environment*, *75*, 305−323.

Moreno-de las Heras, M., Merino-Martín, L., & Nicolau, J. M. (2009). Effect of vegetation cover on the hydrology of reclaimed mining soils under Mediterranean-Continental climate. *Catena*, *77*(1), 139−147.

Morisette, J. T., Richardson, A. D., Knapp, A. K., Fisher, J. I., Graham, E. A., Abatzoglou, J., et al. (2009). Tracking the rhythm of the seasons in the face of global change: phonological research in the 21st century. *Front Ecology Environment*, *7*, 253−260. doi:10.1890/070217.

Mustard, J. F., & Pieters, C. M. (1987). Abundance and distribution of ultramafic microbreccia in moses rock dike-quantitative application of mapping spectroscopy. *Journal of Geophysical Research-Solid Earth and Planets*, *92*(NB10), 10376−10390.

Myneni, R. B., Keeling, C. D., Tucker, C. J., Asrar, G., & Nemani, R. R. (1997). Increased plant growth in the northern high latitudes from 1981–1991. *Nature*, *386*, 698−702.

Nagler, P., Glenn, E., Thompson, T., & Huete, A. (2004). Leaf area index and Normalized Difference Vegetation Index as predictors of canopy characteristics and light interception by riparian species on the Lower Colorade River. *Agricultural and Forest Meteorology*, *116*, 103−112.

Ormsby, J., Choudry, B., & Owe, M. (1987). Vegetation spatial variability and its effect on vegetation index. *International Journal of Remote Sensing*, *8*, 1301−1306.

Purevdorj, T. S., Tateishi, R., Ishiyama, T., & Honda, Y. (1998). Relationships between percent vegetation cover and vegetation indices. *International Journal of Remote Sensing*, *19*, 3519−3535.

Qi, J., Marsett, R. C., Moran, M. S., Goodrich, D. C., Heilman, P., Kerr, Y. H., et al. (2000). Spatial and temporal dynamics of vegetation in the San Pedro River basin area. *Agricultural and Forest Meteorology*, *105*, 55−68.

Ratkowsky, D. A. (1983). *Nonlinear regression modeling—A unified practical approach* (pp. 61−91). New York: Marcel Dekker.

Reed, B. C., Brown, J. F., VanderZee, D., Loveland, T. R., Merchant, J. W., & Ohlen, D. O. (1994). Measuring phenological variablity from satellite imagery. *Journal of Vegetation Science*, *5*, 703−714.

Reed, B. C., Schwartz, M. D., & Xiao, X. (2009). Remote sensing phenology: Status and the way forward. In A. Noormets (Ed.), *Phenology of ecosystem processes: applications in global change research* (pp. 231−246). New York: Springer. doi:10.1007/978-1-4419-0026-5_10.

Richards, F. J. (1959). A flexible growth function for empirical use. *Journal of Experimental Botany*, *10*, 290−300.

Richardson, A. D., Bailey, A. S., Denny, E. G., Martin, C. W., & O'Keefe, J. (2006). Phenology of a northern hardwood forest canopy. *Global Change Biology*, *12*, 1174−1188.

Richardson, A. D., Braswell, B. H., Hollinger, D., Jenkins, J. P., & Ollinger, S. V. (2009). Near-surface remote sensing of spatial and temporal variation in canopy phenology. *Ecological Applications*, *19*(6), 1417−1428.

Román, M. O., Schaaf, C. B., Woodcock, C. E., Strahler, A. H., Yang, X., Braswell, R. H., et al. (2009). The MODIS (Collection V005) BRDF/albedo product: Assessment of spatial representativeness over forested landscapes. *Remote Sensing of Environment*, *113*, 2476−2498.

Schaaf, C. B., Gao, F., Strahler, A. H., Lucht, W., Li, X., Tsang, T., et al. (2002). First operational BRDF, albedo and nadir reflectance products from MODIS. *Remote Sensing of Environment*, *83*, 135−148.

Schaberg, P. G., Van den Berg, A. K., Murakami, P. F., Shane, J. B., & Donnelly, J. R. (2003). Factors influencing red expression in autumn foliage of sugar maple trees. *Tree Physiology*, *23*(5), 325−333.

Schwartz, M. D., & Hanes, J. M. (2009). Intercomparing multiple measures of the onset of spring in eastern North America. *International Journal of Climatology*, *30*(11), 1614−1626.

Schwartz, M. D., & Reiter, B. E. (2000). Changes in North American spring. *International Journal of Climatology*, *20*, 929−932.

Settle, J. J., & Drake, N. A. (1993). Linear mixing and the estimation of ground cover proportions. *International Journal of Remote Sensing*, *14*(6), 1159−1177.

Smith, M. O., Jonson, P. E., & Adams, J. B. (1985). Quantitative determination of mineral types and abundances from reflectance spectra using principle components analysis. *Journal of Geophysical Research*, *80*, 797−804.

Smith, M. O., Ustin, S. L., Adams, J. B., & Gillespie, A. R. (1990). Vegetation in deserts: I. A regional measure of abundance from multispectral images. *Remote Sensing of Environment*, *31*, 1−26.

Tan, B., Woodcock, C. E., Hu, J., Zhang, P., Ozdogan, M., Huang, D., et al. (2006). The impact of gridding artifacts on the local spatial properties of MODIS data: Implications for validation, compositing, and band-to-band registration across resolutions. *Remote Sensing of Environment*, *105*, 98−114.

Thornes, J. B. (1985). The ecology of erosion. *Geography*, *68*, 225−235.

Timmerman, W., Kustas, W., Aderson, M., & French, A. (2007). An intercomparison of the Surface Energ Balance Algorithm for Land (SEBAL) and the Two-Source Energy Balance (TSEB) modeling schemes. *Remote Sensing of Environment*, *108*, 369−384.

Tompkins, S., Mustard, J. F., Pieters, C. M., & Forsyth, D. W. (1997). Optimization of endmembers for spectral mixture analysis. *Remote Sensing of Environment*, *59*, 472−489.

Wan, Z. M., Zhang, Y. L., Zhang, Q. C., & Li, Z. L. (2002). Validation of the land-surface temperature products retrieved from Terra Moderate Resolution Imaging Spectroradiometer data. *Remote Sensing of Environment*, *83*, 163−180.

White, M. A., Thornton, P. E., & Running, S. W. (1997). A continental phenology model for monitoring vegetation responses to interannual climatic variability. *Global Biogeochemical Cycles*, *11*, 217−234.

White, M. A., de Beurs, K. M., Didan, K., Inouye, D. W., Richardson, A. D., Jensen, O. P., et al. (2009). Intercomparison, interpretation, and assessment of spring phenology in North America estimated from remote sensing for 1982–2006. *Global Change Biology*, *15*(10), 2335−2359.

Wittich, K. -P., & Hansing, O. (1995). Area-averaged vegetation cover fraction estimated from satellite data. *International Journal of Biometeorology*, *38*, 209−215.

Xiao, J., & Moody, A. (2005). A comparison of methods for estimating fractional green vegetation cover within a desert-to-upland transition zone in central New Mexico, USA. *Remote Sensing of Environment*, *98*, 237−250.

Zeng, X., Dickinson, R. E., Walker, A., & Shaikh, M. (2000). Derivation and evaluation of global 1-km fractional vegetation cover data for land modeling. *Journal of Applied Meteorology*, *39*, 826−839.

Zhang, X., Drake, N. A., & Wainwright, J. (2002). Scaling land-surface parameters for global scale soil-erosion estimation. *Water Resources Research*, *38*(9), 191−199.

Zhang, X., Friedl, M. A., & Schaaf, C. B. (2006). Global vegetation phenology from MODIS: evaluation of global patterns and comparison with in situ measurements. *Journal of Geophysical Research*, *111*, G04017. doi:10.1029/2006JG000217.

Zhang, X., Friedl, M. A., & Schaaf, C. B. (2009). Sensitivity of vegetation phenology detection to the temporal resolution of satellite data. *International Journal of Remote Sensing*, *30*(8), 2061−2074. doi:10.1080/01431160802549237.

Zhang, X., Friedl, M. A., Schaaf, C. B., & Strahler, A. H. (2004). Climate controls on vegetation phenological patterns in northern mid- and high latitudes inferred from MODIS data. *Global Change Biology*, *10*, 1133−1145.

Zhang, X., Friedl, M. A., Schaaf, C. B., Strahler, A. H., Hodges, J. C. F., Gao, F., et al. (2003). Monitoring vegetation phenology using MODIS. *Remote Sensing of Environment*, *84*, 471−475.

Zhang, X., Tarpley, D., & Sullivan, J. (2007). Diverse responses of vegetation phenology to a warming climate. *Geophysical Research Letters*, *34*, L19405. doi:10.1029/2007GL031447.